ChemElectroChem

Research Article
doi.org/10.1002/celc.202201109

Chemistry Europe
European Chemical Societies Publishing

www.chemelectrochem.org

Interactions between Hydrogen and Palladium Nanoparticles: Resolving Adsorption and Absorption Contributions

Lilian Moumaneix, Akseli Rautakorpi, and Tanja Kallio*[a]

Despite the apparent simplicity of palladium hydride systems, interactions between hydrogen and palladium are multifaceted. Electrochemical hydrogen stripping allows measuring the stoichiometric coefficient of hydrogen atoms inside PdH_x structures, whose properties greatly depend on *x*. In this paper, the insertion of H into Pd nanoparticles has been studied in a three-electrode setup (RDE) and a proton pump cell. An original way of modelling the hydrogen desorption curve is proposed, helping in the separation of hydrogen absorption from other contributions. The loading voltage exhibits the highest impact on the H absorption into Pd, reaching H_{abs}/Pd up to 0.47 ± 0.02 in the RDE setup, at $-0.2\ V_{RHE}$. Conversely, the loading duration presents only little influence in the very first seconds. Finally, maximal H_{abs}/Pd ratios are measured around 30–40 °C, likely due to an optimal balance between the H adsorption rate, and the H diffusion rate into Pd.

Introduction

Palladium has been thoroughly studied for its remarkable behaviour in presence of hydrogen. Due to its ability to absorb large volumetric quantities of hydrogen under ambient conditions, Pd has been investigated for many hydrogen-related applications, including hydrogen storage or enhanced spillover,[1–3] hydrogen purification,[4–8] hydrogen sensors,[9–11] or catalysis purposes.[12–14] Other applications that take advantage of changes in the electrical,[15] magnetic, mechanical, and/or optical properties of palladium hydride could also be considered in the future.

Palladium crystallizes in a face-centred cubic structure with four octahedral and eight tetrahedral interstitial sites per unit cell. Before forming a metal-hydride system, protons undergo an adsorption process according to the Volmer reaction (eq. 1), hereafter in acidic media:

$$H^+ + Pd + e^- \rightleftarrows PdH_{ads} \quad (1)$$

Where *Pd* is the adsorption site and PdH_{ads} is the hydrogen atom adsorbed on the palladium surface. Under standard conditions, two distinct phenomena are differentiated: (i) the under-potential deposition of hydrogen (HUPD), taking place at potentials more positive than the thermodynamic reversible potential of the hydrogen evolution reaction (E^0_{HER}), i.e. 0 V vs RHE; (ii) the over-potential deposition of hydrogen (HOPD), taking place at potentials below E^0_{HER}. The HUPD is characteristic of a very limited category of noble metals, including Pt, Rh, Ir, and Pd. HOPD is described as the intermediate species to the hydrogen evolution reaction (HER).[16]

It is generally accepted that the absorption of hydrogen in the palladium bulk presents an intermediary stage where hydrogen atoms are located in subsurface positions (eq. 2):[17]

$$PdH_{ads} + Pd_{sub} \rightleftarrows Pd_{surface} + PdH_{sub} \quad (2)$$

Afterwards, hydrogen atoms are expected to diffuse in the palladium bulk by jumping from one octahedral site to another (eq. 3):[18]

$$PdH_{sub} \rightleftarrows Pd_{abs} \quad (3)$$

In parallel to the absorption process, adsorbed hydrogen can also react to form gaseous dihydrogen following two different paths, (i) the Heyrovsky reaction (eq. 4), i.e. electrochemical desorption or electroreduction:

$$PdH_{ads} + H^+ + e^- \rightleftarrows Pd + H_2 \quad (4)$$

(ii) the Tafel reaction (eq. 5), i.e. non-electrochemical removal or recombination:

$$2PdH_{ads} \rightleftarrows 2Pd + H_2 \quad (5)$$

Some studies also proposed a direct absorption of hydrogen, from the electrolyte to a subsurface position.[19,20] This has been experimentally evidenced by poisoning the surface of Pd thin films with crystal violet, which does not hinder the H absorption even though H adsorption is greatly reduced.[21] The overall mechanism may involve both direct and indirect absorption of hydrogen in unknown proportions, even if the

[a] Dr. L. Moumaneix, A. Rautakorpi, Prof. T. Kallio
Department of Chemistry and Materials Science
Aalto University
Espoo, 00076 Aalto (Finland)
E-mail: tanja.kallio@aalto.fi

Supporting information for this article is available on the WWW under https://doi.org/10.1002/celc.202201109

ChemElectroChem

Research Article
doi.org/10.1002/celc.202201109

Chemistry Europe
European Chemical Societies Publishing

www.chemelectrochem.org

Interactions between Hydrogen and Palladium Nanoparticles: Resolving Adsorption and Absorption Contributions

Lilian Moumaneix, Akseli Rautakorpi, and Tanja Kallio*[a]

Despite the apparent simplicity of palladium hydride systems, interactions between hydrogen and palladium are multifaceted. Electrochemical hydrogen stripping allows measuring the stoichiometric coefficient of hydrogen atoms inside PdH_x structures, whose properties greatly depend on *x*. In this paper, the insertion of H into Pd nanoparticles has been studied in a three-electrode setup (RDE) and a proton pump cell. An original way of modelling the hydrogen desorption curve is proposed, helping in the separation of hydrogen absorption from other contributions. The loading voltage exhibits the highest impact on the H absorption into Pd, reaching H_{abs}/Pd up to 0.47 ± 0.02 in the RDE setup, at -0.2 V_{RHE}. Conversely, the loading duration presents only little influence in the very first seconds. Finally, maximal H_{abs}/Pd ratios are measured around 30–40 °C, likely due to an optimal balance between the H adsorption rate, and the H diffusion rate into Pd.

Introduction

Palladium has been thoroughly studied for its remarkable behaviour in presence of hydrogen. Due to its ability to absorb large volumetric quantities of hydrogen under ambient conditions, Pd has been investigated for many hydrogen-related applications, including hydrogen storage or enhanced spillover,[1–3] hydrogen purification,[4–8] hydrogen sensors,[9–11] or catalysis purposes.[12–14] Other applications that take advantage of changes in the electrical,[15] magnetic, mechanical, and/or optical properties of palladium hydride could also be considered in the future.

Palladium crystallizes in a face-centred cubic structure with four octahedral and eight tetrahedral interstitial sites per unit cell. Before forming a metal-hydride system, protons undergo an adsorption process according to the Volmer reaction (eq. 1), hereafter in acidic media:

$$H^+ + Pd + e^- \rightleftarrows PdH_{ads} \quad (1)$$

Where *Pd* is the adsorption site and PdH_{ads} is the hydrogen atom adsorbed on the palladium surface. Under standard conditions, two distinct phenomena are differentiated: (i) the under-potential deposition of hydrogen (HUPD), taking place at potentials more positive than the thermodynamic reversible potential of the hydrogen evolution reaction (E^0_{HER}), i.e. 0 V vs RHE; (ii) the over-potential deposition of hydrogen (HOPD), taking place at potentials below E^0_{HER}. The HUPD is characteristic of a very limited category of noble metals, including Pt, Rh, Ir, and Pd. HOPD is described as the intermediate species to the hydrogen evolution reaction (HER).[16]

It is generally accepted that the absorption of hydrogen in the palladium bulk presents an intermediary stage where hydrogen atoms are located in subsurface positions (eq. 2):[17]

$$PdH_{ads} + Pd_{sub} \rightleftarrows Pd_{surface} + PdH_{sub} \quad (2)$$

Afterwards, hydrogen atoms are expected to diffuse in the palladium bulk by jumping from one octahedral site to another (eq. 3):[18]

$$PdH_{sub} \rightleftarrows Pd_{abs} \quad (3)$$

In parallel to the absorption process, adsorbed hydrogen can also react to form gaseous dihydrogen following two different paths, (i) the Heyrovsky reaction (eq. 4), i.e. electrochemical desorption or electroreduction:

$$PdH_{ads} + H^+ + e^- \rightleftarrows Pd + H_2 \quad (4)$$

(ii) the Tafel reaction (eq. 5), i.e. non-electrochemical removal or recombination:

$$2PdH_{ads} \rightleftarrows 2Pd + H_2 \quad (5)$$

Some studies also proposed a direct absorption of hydrogen, from the electrolyte to a subsurface position.[19,20] This has been experimentally evidenced by poisoning the surface of Pd thin films with crystal violet, which does not hinder the H absorption even though H adsorption is greatly reduced.[21] The overall mechanism may involve both direct and indirect absorption of hydrogen in unknown proportions, even if the

[a] Dr. L. Moumaneix, A. Rautakorpi, Prof. T. Kallio
Department of Chemistry and Materials Science
Aalto University
Espoo, 00076 Aalto (Finland)
E-mail: tanja.kallio@aalto.fi

Supporting information for this article is available on the WWW under https://doi.org/10.1002/celc.202201109

kinetic rate of the direct absorption has been proposed to be faster than the indirect one. Figure 1 gathers the different reactions taking place on a Pd nanoparticle (NP) in contact with protons.

It is well known that palladium hydride PdH_x can be found in at least three different phases, depending on the proportion of hydrogen present in its structure. For $x < 0.05$, PdH_x constitutes a solid solution named α phase. Between approximately $0.05 < x < 0.7$, PdH_x is constituted of a mix between the α and β phases. Above $x = 0.7$, the β phase is suggested to be the only one remaining. An additional γ phase is more rarely considered, which could start appearing for $x > 0.7$, mixed with the β phase.[22–24]

The hydrogen loaded into the Pd lattice, often presented as the molar H/Pd ratio, is a critical parameter to estimate, as many properties of the PdH_x-system vary with x. Several ways to measure the H/Pd ratio have been presented throughout the years, based on different properties of the PdH_x system, e.g. increase in resistivity, mass, and lattice parameters. More recently, electrochemical methods have been widely used, mostly based on recording hydrogen desorption at a constant potential. However, each technique has its pros and cons, and limitations that are worth considering.

The resistance ratio method has been used for many decades and takes advantage of the dependence of PdH_x electrical resistivity on hydrogen concentration, which shows a maximum at $x \approx 0.7$.[22,25,26] However, above this concentration the PdH_x resistivity decreases, thus implying the existence of two possible compositions for the same resistivity ratio. In addition, the PdH_x resistivity is greatly influenced by external physical parameters, e.g. temperature variations. Nonetheless, this technique is a fairly simple way to estimate the H/Pd ratio *in situ*.[27]

The gravimetric method utilizes the increase in mass between PdH_x and bare Pd electrode. Rarely encountered in the literature, this approach takes a significant amount of time to be carried out, as results should be repeated several times for higher accuracy.[28] Some limitations arise from the use of this method, (i) only bulk electrodes can be weighted with sufficient accuracy to determine the mass difference, thus implying long loading durations; (ii) hydrogen atoms start to naturally recombine as soon as the loading potential is turned off, leading to underestimating results; (iii) while outside of the electrolyte, the electrode can be affected by the ambient atmosphere, e.g. undergo water adsorption.

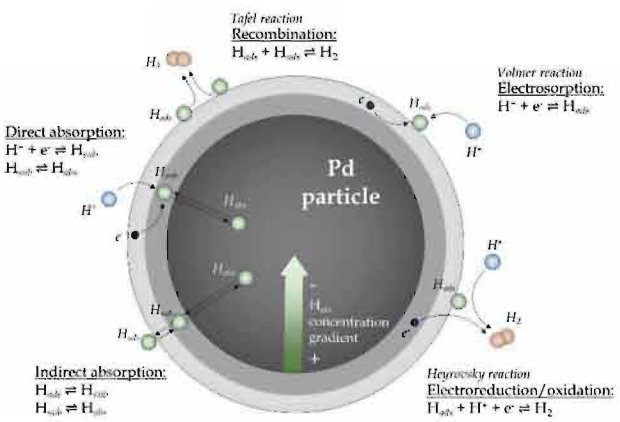

Figure 1. Overview of the reactions involving hydrogen atoms at a palladium-based electrode submitted to potentials below 0 V_{RHE}.

In operando measurements of the PdH_x lattice parameters using X-ray diffraction (XRD) has been shown to be one of the most accurate techniques to measure the H/Pd ratio. When hydrogen atoms are inserted into the interstitial positions of the Pd lattice, an expansion of the lattice parameters is observed.[29–31] Yet, access to this method is made difficult by the unconventional electrochemical cells that it demands and the availability of high energy x-ray beams, such as in the synchrotron facilities, necessary to analyse the inside of the cell under operation with a fast time resolution.

The coulometric stripping method is widely used in the literature to quantify the quantity of hydrogen adsorbed onto the Pd surface and absorbed inside the bulk of the material. Commonly, this method is used in a three-electrode setup, with the palladium catalyst deposited on the working electrode. A potential negative enough to load the palladium with hydrogen is applied, typically around -0.1 V_{RHE}, before switching the applied potential to a value positive enough to observe the desorption of hydrogen, typically between 0.4 V_{RHE} and 0.65 V_{RHE}.[32–34] This *in situ* method is easy to set up, allows a wide variety of small-volume setups as well as a wide variety of materials (nanoparticles, thin films, wires), and does not demand calibration or complex instrumentation. Additionally, this technique is usually quite fast, i.e. a few minutes, is sensitive, and allows many different sets of experimental conditions, e.g. different temperatures, feeding gases, gas contaminants.[24,31–36] The overall quantity of hydrogen atoms stored onto or into the palladium structure is calculated by integrating the current passed during the desorption step. However, a significant contribution from the hydrogen oxidation reaction (HOR) is also part of the desorption curves, due to the presence of evolved H_2 in the WE surroundings or trapped into its microstructure, resulting in an overestimation of the H/Pd ratios. Some research works have been focusing on limiting the contribution of the HOR, with for example the use of an electrochemical flow cell to displace hydrogen bubbles from the surface of the WE.[33] It was also shown that bubbling the electrolyte with an inert gas and/or using a rotating disk electrode is an efficient way to greatly decrease the accumulation of H_2 on the WE and thus, limiting its oxidation during the desorption step.[21]

In earlier studies, the group of Lasia *et al.* has proposed a method to separate the contributions of H adsorption and H absorption in Pd thin films (20–80 nm).[37,38] It was revealed that for increasing film thicknesses, if the hydrogen adsorption is similar (and only related to the electrode surface area), the absorption represents an increasing portion of the total charge during the desorption. However, no investigation was carried out in the case of Pd nanoparticles (NPs), for which the direct estimation of the surface phenomena is hindered by the use of a support material, which contributes to the double-layer capacitance. The group of Czerwinski *et al.* studied the

adsorption and absorption of H on and in Pd thin films grown on Au in presence of CO.[39,40] After saturating the Pd sample with H, CO can be injected, which results in a positive oxidation current that the authors attributed to the oxidation of H as it is replaced by CO molecules.[39] However, it stays unclear what proportion of the adsorbed H goes undetected by this method as some atoms undergo a non-electrochemical removal.

In this paper, we propose an original and easy way to decompose the desorption curves recorded during coulometric stripping analysis, to extract the contribution from the hydrogen actually absorbed into the palladium lattice. Additionally, H absorption has been performed in both liquid electrolyte and proton pump setup, the latter allowing to reach much lower voltages, up to −0.5 V, and thus exploring a region rarely studied. An extensive investigation of the influence of the loading voltage, the loading duration, and the setup temperature on the absorption of H into Pd NPs has been carried out, leading to a better comprehension of the overall mechanisms. Pd NPs have been preferred to Pd thin films due to their extensive use in numerous applications, especially in the field of electrocatalysis, e.g. CO_2 reduction, where their size and composition play a very significant role in the reaction mechanism.

Results and discussion

Modelling of the desorption curves

The desorption curves recorded at constant potential (+0.4 V) have been modelled following a simple procedure, based on the diffusion of different hydrogen species to the surface of Pd particles and their subsequent desorption in the form of protons and electrons through either the Volmer and/or Heyrovsky reactions. The resulting current is thereafter compared with the experimental data.

For the sake of simplicity, reactions occurring during the desorption process are assumed to be of the first order. This assumption is based on fundamental studies which showed that the desorption of H atoms from Pd (100) follows a quasi-first-order kinetics.[41] However, for low H coverage, the H desorption is a second-order reaction, which might explain some small discrepancies between the model and experimental data at low current densities. In addition, it was established that the migration of H atoms on the Pd surface, i.e. due to an electric field gradient, is a first-order reaction, which also supports the decision to use first-order kinetics for the diffusion of hydrogen atoms to the Pd surface. Additionally, as the potential difference applied acts as a driving force towards the desorption of H_{ads}, the following reactions are assumed to be non-reversible.

Three couples of reactions are first considered (cf. Figure 2), describing the two-step diffusion to the Pd surface of (i) hydrogen atoms absorbed into the Pd lattice, (ii) hydrogen atoms adsorbed on the surrounding carbon support (hydrogen spillover) and (iii) dihydrogen in the vicinity of Pd NPs, evolved during the electrochemical loading step. As the surface of Pd NPs is limited and firstly occupied by adsorbed hydrogens, these two-step reactions have been used to express the existence of intermediary "buffer" positions from which hydrogen atoms can readily react to form adsorbed hydrogens.

In parallel, adsorbed hydrogen atoms undergo desorption according to the Volmer reaction (eq. 6):

$$H_{ads} \xrightarrow{k_7} H^+ + e^- \quad (6)$$

Three sets of equations are used to calculate the quantity of each species at a specific time. The decrease in the quantity of species in a "bulk" position (noted $[H_{bulk}]$), i.e. appliable for H_{abs}, $H_{2,\,bulk}$ and H_{spIII}, is calculated according to equations 7 and 8. The general reaction rate constant k_n must be replaced by the corresponding one from Figure 2. Δt corresponds to the

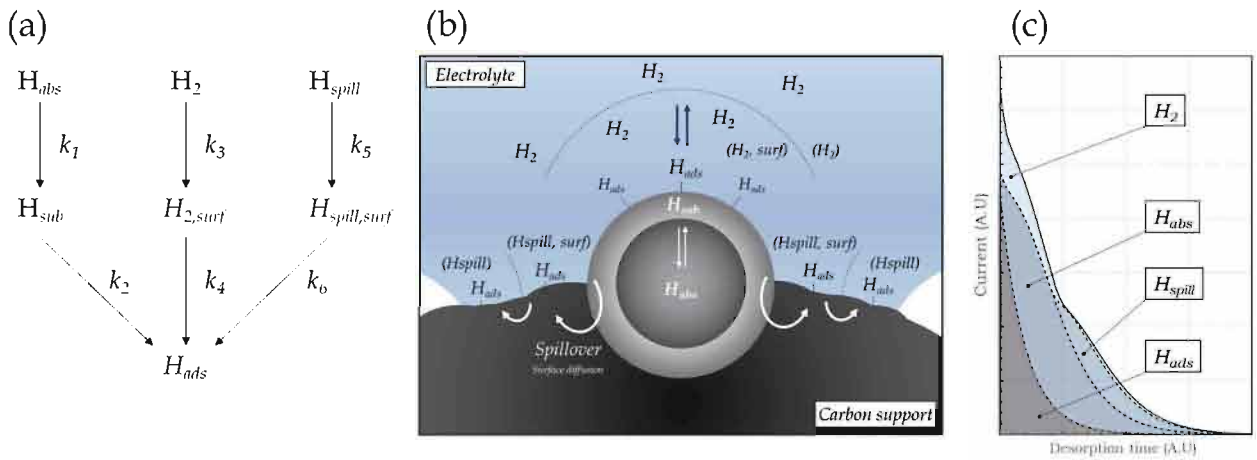

Figure 2. (a) Reactions considered in the modelling of the electrochemical desorption curves, k_x indicate the reaction rate constants; (b) scheme summarizing the different positions for hydrogen atoms considered in the model and (c) their impacts on a typical desorption curve.

time difference between two successive points (in s), which are respectively indicated with the subscripts (t-1) and (t).

$$\frac{d[H_{bulk}]}{dt} = -k_n[H_{bulk}]_{(t)} \tag{7}$$

$$[H_{bulk}]_{(t)} = \exp\left[-k_n\Delta t + ln\left([H_{bulk}]_{(t-1)}\right)\right] \tag{8}$$

The quantity of intermediary species (noted $[H_{inter}]$), i.e. appliable for H_{sub}, $H_{2,surf}$ and $H_{spIII,surf}$, both increases and decreases due to the diffusion of bulk species and the formation of H_{ads} respectively. The overall change is calculated as follows (eq. 9 and 10), where k_m should be replaced by the corresponding reaction rate constant from Figure 2:

$$\frac{d[H_{inter}]}{dt} = k_n[H_{bulk}]_{(t)} - k_m[H_{inter}]_{(t)} \tag{9}$$

$$[H_{inter}]_{(t)} = \frac{k_n[H_{bulk}]_{(t)}}{k_m} + \left([H_{inter}]_{(t-1)} - \frac{k_n[H_{bulk}]_{(t)}}{k_m}\right)e^{-k_m\Delta t} \tag{10}$$

The amount of H_{ads} is depending on the rate at which it is consumed to form H^+, as well as the rates at which the intermediary species participate in the replenishment of this adsorbed layer. The change in quantity can be calculated according to equations 11 and 12:

$$\frac{d[H_{ads}]}{dt} = k_2[H_{sub}]_{(t)} + 2k_4[H_{2,surf}]_{(t)} + k_6\left[H_{spill,surf}\right]_{(t)} - k_7[H_{ads}]_{(t)} \tag{11}$$

$$[H_{ads}]_{(t)} = \frac{k_2[H_{sub}]_{(t)} + 2\,k_4\left[H_{2,surf}\right]_{(t)} + k_6\left[H_{spill,surf}\right]_{(t)}}{k_7} + \left([H_{ads}]_{(t-1)} - \frac{k_3[H_{sub}]_{(t)} + 2\,k_3\left[H_{2,surf}\right]_{(t)} + k_6\left[H_{spill,surf}\right]_{(t)}}{k_7}\right) e^{-k_7\Delta t} \tag{12}$$

Finally, the current resulting from the whole process can be computed by assuming that each H_{ads} atom reacts to give one electron. Therefore, it is possible to convert the molar quantities of desorbed hydrogen into an equivalent number of electrons, leading to the following equation 13, considering all the replenishments described in the model:

$$[e^-]_{(t)} = \Delta[H_{ads}]_{(t-1)-t} + \Delta[H_{abs}]_{(t-1)-t} + \Delta[H_{sub}]_{(t-1)-t} \cdot 2\Delta[H_2]_{(t-1)-t} + 2\Delta\left[H_{2,\,surf}\right]_{(t-1)-t} \cdot \Delta\left[H_{spill}\right]_{(t-1)-t} \cdot \Delta\left[H_{spill,surf}\right]_{(t-1)-t} \tag{13}$$

Where $\Delta[X]_{(t-1)-t}$ is the molar quantity difference of the specie X between two successive points at *(t-1)* and *t*.

The resulting current can be calculated with equation 14:

$$i_{(t)} = \frac{[e^-]_{(t)} \times q_e}{\Delta t} \tag{14}$$

To provide a good fit of the data, the availability of the Pd surface had to be considered in the case of the spillover contribution, as H atoms cannot diffuse from the carbon surface to any available position on the Pd surface. It is proposed that only a fraction of the Pd surface is accessible to H_{spIII} diffusion, describing that only a fraction of the Pd NP surface is directly in contact with its support. To represent this behaviour, a coverage parameter has been introduced, ranging from 0 to 1. When multiplied by the initial quantity of H_{ads}, i.e. when the surface is saturated, it gives a maximum limit above which the surface is not considered available for H_{spIII} diffusion. Coverage values were determined from the current derivative curves, by centring the calculated peak associated with the spillover contribution with respect to the experimental data. An example is provided in S.I. 2. Typical coverage values were found between 0.3 and 0.5.

In addition, it is considered that the quantity of H_{ads} at all times cannot surpass its initial value ($H_{ads,0}$), which is assumed to correspond to the saturation of the Pd surface with H atoms. In case of over-saturation, the difference between the actual amount of H_{ads} and $H_{ads,0}$ is given back to H_{sub}, $H_{spill,surf}$ and/or $H_{2,surf}$, depending on the contributions participating at this specific moment.

The initial parameters of the model, i.e. initial quantities $[H_{bulk}]$ and $[H_{inter}]$, and the reaction rate constant k_x, are optimized using the solver function of Excel by minimizing the absolute difference between experimental and calculated data. In practice, the initial quantities of intermediary species, i.e. $[H_{sub}]_0$, $[H_{2,surf}]_0$, $[H_{spill,surf}]_0$, were kept equal to 0, reducing the number of variables in the model. This simplification of reality is still pertinent as few H atoms are in direct contact with the Pd surface in the very first instants. For all the other parameters, the values were first manually inserted in the model and then allowed to be modified during the optimization. No specific boundaries in addition to the one described before were necessary to perform the fitting. The sensitivity of the model was tested in a ±10% range around the optimized parameters and the resulting errors are represented thereafter by coloured areas around the calculated contributions.

Electrochemical analysis of the proton pump

Proton pumps, often referred to as electrochemical hydrogen compressors, are generally used to purify and pressurize H_2 up to several hundred bars.[42–44] Additionally, they allow a more precise evaluation of the anode material performances in comparison to fuel cells, by removing the contribution coming from the sluggish oxygen reduction reaction.[45] In this work, a proton pump setup has been chosen to study the absorption of protons into Pd at the cathode, without limiting the available voltage range compared to symmetrically fed setups (H_2/H_2) in which measures can only be performed at open circuit voltage (OCV).[46]

In a proton pump configuration, the fuel cell setup is fed with H_2 on the anode side, where it gets oxidized (HOR) before crossing the proton conducting membrane (Nafion) and reach-

ing the cathode where it is reduced back to H_2 (HER). The cathode compartment is constantly flush with N_2, which hinders the accumulation of H_2. In addition to HER, other reactions can occur at the cathode, such as the adsorption and absorption of hydrogen into Pd. In our case, the pressure in both anodic and cathodic compartments was equal to the atmospheric pressure. The potential of each electrode can be calculated in theory with the Nernst equation (eq. 15):

$$E_{th} = E^0_{H^+/H_2} - \frac{RT}{2F} ln \frac{P_{H_2}}{c^2_{H^+}} \quad (15)$$

With $E^0_{H+/H2}$ the standard reduction potential (0 V_{RHE}), R the universal gas constant, F the Faraday constant, P_{H2} the partial pressure of H_2 at the electrode and c^2_{H+} the square of the proton concentration at the electrode. If the theoretical potential of the anode is well-defined, the one of the cathode is more difficult to predict as the partial pressure of H_2 on this side is not set nor constant. However, it can be assumed that the partial pressure of H_2 on the cathodic side is always lower than the one on the anodic side when no current is flowing through the cell, which leads to a positive OCV (E_C-E_A), usually measured around 0.1 V in our setup. The OCV should get closer to 0 V as the partial pressure on the cathodic side approaches the one on the anodic side.

The proton pump shows a remarkably stable behaviour in a large voltage range, typically up to −1 V, as compared with RDE setups in which the HER occurring at the WE surface brings instability below −0.2 V_{RHE}. Thus, proton pump appears to be an interesting alternative for the study of hydrogen absorption at low voltages. Linear sweep voltammetry (LSV) measurements carried out in the proton pump show a typical behaviour (Figure 3(a)), including a short activation region between OCV (0.13 ± 0.01 V) and 0 V, followed by a linear ohmic regime, before reaching a mass transfer limitation below about 0.8 V. Several LSV were always performed prior to absorption/desorption studies, to roughly evaluate the voltage range in which these measures can be done.

Figure 3(b, c) reveals that the mass activity is much higher in the RDE setup compared to the proton pump, which could originate from the lower Pd loading on the WE, ca. 0.116 $mg_{Pd}.cm^{-2}$ and 0.5 $mg_{Pd}.cm^{-2}$ respectively, resulting in thinner catalyst layers and better availability of the Pd NPs. Nonetheless, the same reactions are observed in both setups, (i) hydrogen desorption from absorbed and adsorbed positions at 0.09 V_{RHE} and 0.27 V_{RHE} respectively, (ii) hydrogen adsorption at 0.23 V_{RHE}, (iii) hydrogen absorption starting from 0.05 V_{RHE} and (iv) HER below about 0 V_{RHE}. An additional contribution in the RDE setup appears due to HOR, located between 0–0.05 V_{RHE} in the scan towards positive potentials. This reaction is usually not seen in the proton pump due to the N_2 flushing the cathode and greatly limiting the accumulation of H_2 on this side.

Potentiostatic electrochemical impedance spectroscopy (EIS) has been carried out to better apprehend the limitations of the proton pump at various voltages. The Bode plots displayed in Figure 4(a) exhibit two main contributions attributed to the anodic charge transfer (HOR, (i)) and the cathodic charge transfer (H adsorption, (ii)). Both contributions shift towards higher frequencies as the cell voltage is decreased, due to the faster transfer of electrons at higher current densities. A third peak is visible at low frequency (iii) for the lowest voltages investigated, attributed to increasing mass transfer.

EIS data were modelled using a modified Randles model. Errors in the modelling have been calculated and are below 1%. Figures 4(b) and (c) reveal that at high voltages (> 0 V), the charge transfer at the cathode is significantly higher than the one at the anode, which could be attributed to the low amount of protons crossing the membrane at voltages close to OCV. Nonetheless, the cathodic charge transfer resistance exhibits a rapid decrease with decreasing voltage, much faster

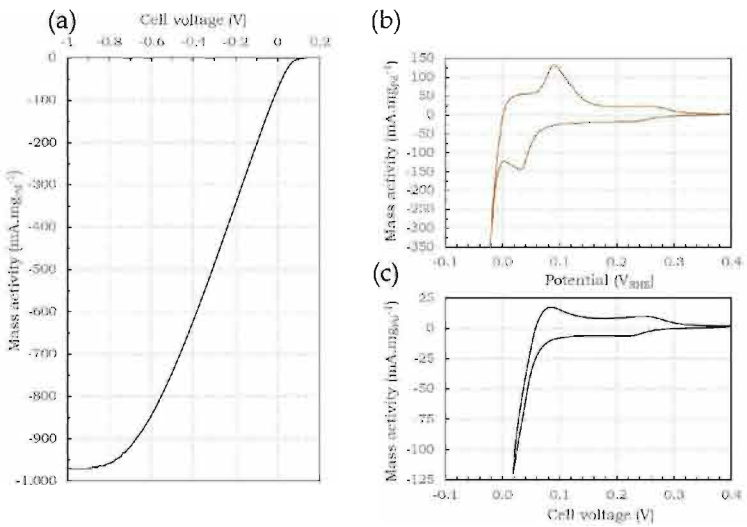

Figure 3. (a) Linear sweep voltammetry of $Pt_{(a)}/Pd_{(c)}$-based MEA in proton pump setup (H_2 and N_2 flowrates 50 mL.min^{-1}, 30 °C, 5 mV.s^{-1}); cyclic voltammetry of (b) Pd/C-based catalyst material in the RDE setup (2500 rpm, 25 °C, 25 mV.s^{-1}, H_2SO_4 0.5 M, iR-corrected) and (c) $Pt_{(a)}/Pd_{(c)}$-based MEA in proton pump setup (H_2 and N_2 flowrates 50 mL.min^{-1}, 30 °C, 25 mV.s^{-1}, iR-corrected).

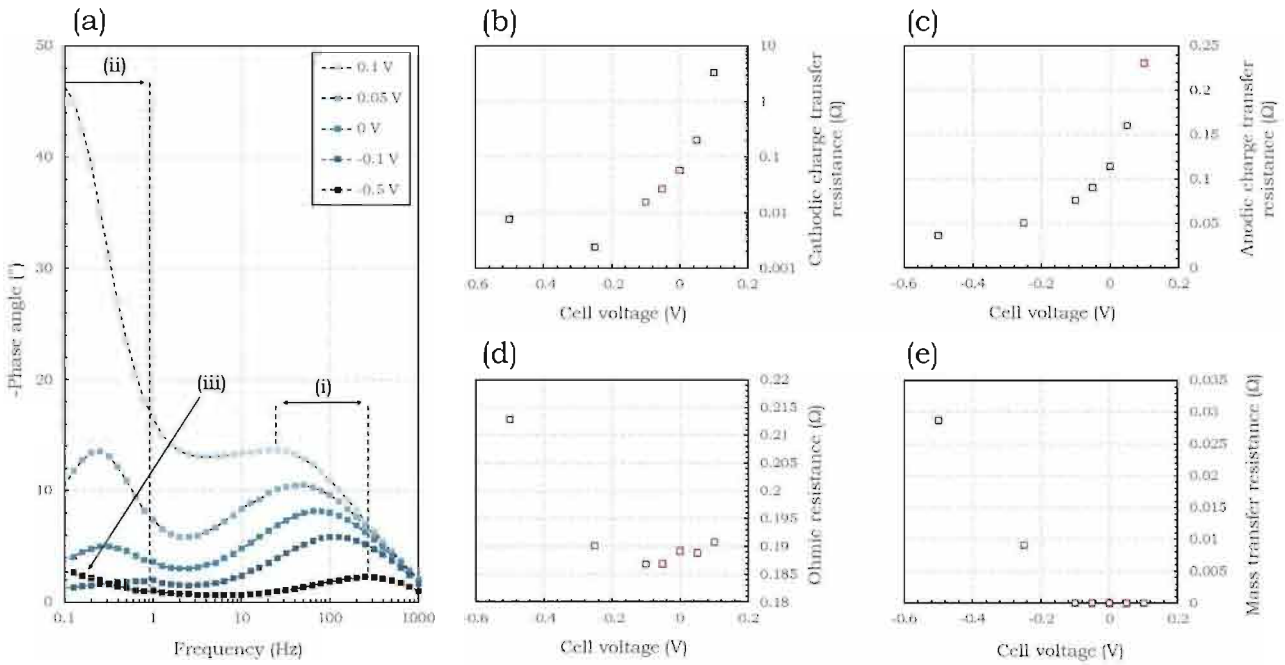

Figure 4. Bode plots obtained from EIS carried out in the proton pump (H_2 and N_2 flowrates 50 mL.min^{-1}, 30 °C), 20 min of stabilization at set potential, 20 mV fluctuations (a). Anodic (i) and cathodic (ii) charge transfer regions are highlighted as well as the mass transfer region (iii). Cathodic charge transfer resistance (b), anodic charge transfer resistance (c), ohmic resistance (d) and mass transfer resistance (e) extracted from the modelling of EIS data with a modified Randles model.

than the anodic one. This behaviour could be attributed to the absence of H_2 on the cathodic side (or a very small quantity), which implies that a decrease in the cell voltage would mostly impact the cathode potential as compared to the anode, whose potential is defined by the Nernst equation (Eq. 15).[45] The cell ohmic resistance, mostly related to the ionic conductivity of the Nafion membrane, shows a slight decrease from 0.1 V to −0.15 V, followed by a significantly larger increase below −0.15 V (Figure 4(d)). This behavior may be attributed to the transport of water molecules along with protons throughout the MEA, which keeps the Nafion membrane well-humidified and highly conductive, until reaching a point where the transport is so large that the anodic side of the membrane starts showing signs of dehydration, leading to an overall increase of the ohmic resistance.[47] Additionally, a mass transfer contribution was measured for voltages below −0.25 V (Figure 4(e)). This mass transfer is likely due to the limited flow of H_2 injected in the system (15–20% decrease at −0.5 V when H_2 flowrate is doubled), as well as the diffusion rate of protons through the Nafion membrane.

Influence of the experimental parameters on the hydrogen absorption into Pd

Influence of the loading potential

The loading potential has been investigated in the ranges from 0.2 V_{RHE} to −0.2 V_{RHE} in the RDE setup and up to −0.5 V in the proton pump. The lower potential limit is higher in the RDE setup due to the formation of a consequent amount of H_2, which cannot be efficiently removed from the WE even at a high rotation speed. In the proton pump, flushing the cathodic side with N_2 prevents the accumulation of the evolved H_2 and allows to carry on the measures at lower voltages.

A reference catalyst material containing commercial Pt NPs on carbon black has been tested in the RDE setup (Figure 5(a)) to compare the results from the desorption curves in absence of hydrogen absorption. At high loading voltages ($E > 0.2$ V_{RHE}), the desorption curves present a regular decay corresponding to the desorption of adsorbed hydrogen from the Pt surface. For $E \leq 0.2$ V_{RHE}, a shoulder in the curve marks the presence of a second H species, interpreted afterwards as hydrogen atoms spilt on the carbon support. Below 0 V_{RHE}, H_2 oxidation becomes visible at the very beginning of the desorption curve, in the form of an additional smaller shoulder (cf. S.I. 3). After modelling (Figure 5(d)), it comes out that the contribution from H_{ads} increases almost linearly as the cell voltage is made more negative and reaches a maximum around 0 V_{RHE} corresponding to H_{ads}/Pt of 0.13 ± 0.02. It should be noted that this ratio considers all the Pt contained in the catalyst layer, and not only the Pt atoms on the surface. The hydrogen spillover contribution follows a similar trend, reaching its maximum around 0 V_{RHE} corresponding to H_{spill}/Pt of 0.07 ± 0.01. Further increase in the total H/Pt ratio when polarized below 0 V_{RHE} comes almost exclusively from the oxidation of H_2, evolved during the loading step, up to H_2/Pt of 0.04 ± 0.01.

In the case of the Pd-based catalyst material, the desorption curves from the RDE tests (Figure 5(b)) exhibit a very pronounced change in their aspect as the loading

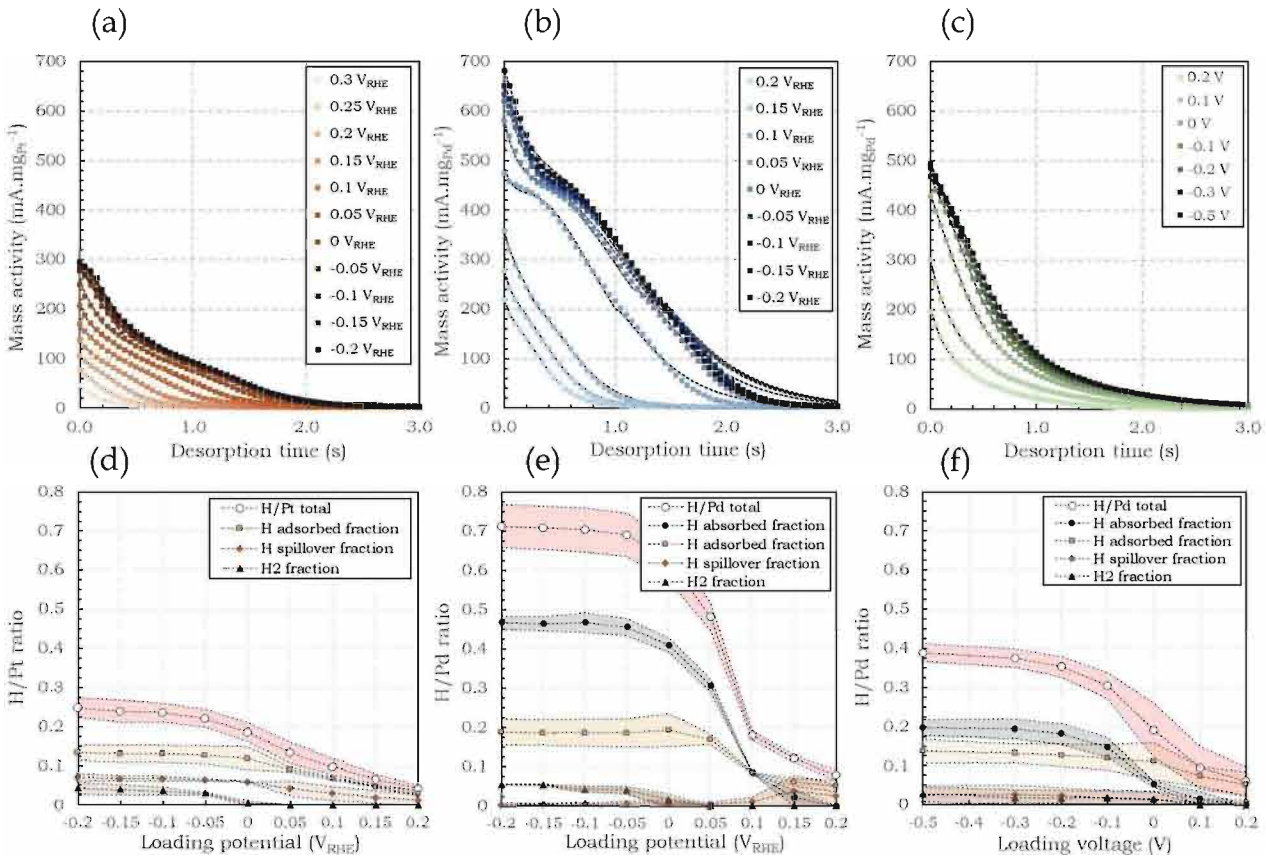

Figure 5. Electrochemical desorption curves recorded after 60 s loading at the specified cell voltage, desorption at +0.4 V and calculated contributions of the different hydrogen species. (a, d) Pt/C-based catalyst material in the RDE setup (2500 rpm, 25 °C, H_2SO_4 0.5 M), (b, e) Pd/C-based catalyst material in the RDE setup (2500 rpm, 25 °C, H_2SO_4 0.5 M) and (c, f) $Pt_{(a)}/Pd_{(c)}$-based MEA in the proton pump setup (H_2 and N_2 flowrates 50 mL.min^{-1}, 30 °C). The dotted lines on the desorption curves correspond to the calculated model. Coloured areas correspond to the experimental error based on two (d and e) or four (f) different measurements under similar conditions.

potential is made more negative. At high loading voltages ($E >$ 0.1 V_{RHE}), the desorption curves present the same behaviour as with Pt, corresponding to the desorption of adsorbed hydrogen atoms, as well as a smaller contribution attributed to the desorption of hydrogen spillover. In accordance with the cyclic voltammetry (CV) measurements, from 0.05 V_{RHE} and below, a third contribution related to the desorption of absorbed hydrogen atoms appears in the form of a second prominent shoulder. This sudden change corresponds to the formation of the β-PdH_x after which the system tends to stabilize. More information about the visualization and attribution of the contributions is available in S.I. 3–5. In the proton pump setup (Figure 5(c)), the desorption curves show the same behaviours, but the shoulders are more difficult to discern. Due to the constant nitrogen flushing of the cathode, a part of the hydrogen atoms could be constantly removed from the catalyst layer, leading to lower local hydrogen quantities overall.

The modelling of the desorption curves gives additional information on the number of hydrogen atoms involved in each contribution (Figure 5(e, f)). In the same way as with Pt, hydrogen adsorption (HUPD) seems to reach a plateau around 0 V_{RHE}, up to H_{ads}/Pd ratios of 0.19 ± 0.03 and 0.14 ± 0.03 for the RDE and proton pump setups respectively. Close values were expected as the commercial Pd NPs should present the same surface area in both catalyst layers. The slightly higher values measured in the RDE setup could be explained by: (i) the thinner catalyst layer in this configuration, enhancing the availability of the Pd surface and (ii) a lower amount of Nafion ionomer in the catalyst layer, which could get adsorbed on the Pd surface at positive cathode potentials, decreasing the available surface for H adsorption. Below 0 V_{RHE}, most of the Pd surface is covered with H atoms, and further adsorption (HOPD) leads to HER.

Hydrogen absorption starts at 0.1 V_{RHE} and follows a steep increase before reaching a plateau around −0.1 V_{RHE} and −0.2 V in the RDE and proton pump setups respectively. The number of hydrogen atoms inserted into the Pd lattice varies greatly between the two setups, with H_{abs}/Pd ratios of about 0.20 ± 0.02 in the proton pump and up to 0.47 ± 0.02 in the RDE setup. The transition from the α-PdH_x phase to the β-PdH_x phase occurs between 0.1 V_{RHE} and 0.05 V_{RHE}, in good agreement with earlier experimental observations.[24,35,36] A H_2 concentration gradient between the solid phase (catalyst layer) and the gas phase (N_2) could explain the lower H_{abs}/Pd ratio in the proton pump, as it implies the displacement of a

part of the H_{abs} onto the Pd surface to form H_2 to counteract the established gradient. Despite its impact on the results, flushing the cathode is a necessary condition to obtain understandable electrochemical desorption curves. In absence of gas flowing in the cathodic compartment, the amount of H_2 in the setup would dramatically increase and make pertinent characterizations considerably more difficult to achieve.

The fraction of spillover H is small in regard to the adsorption on Pd NPs. This contribution is present even at high loading voltages, but its overall quantity remains small over the voltage range investigated, which makes difficult any in-depth analysis. As could be expected, the contribution from evolved H_2 appears below 0 V_{RHE} and represents most of the increase in the total H/Pd(Pt) ratio below this same voltage. The contribution quickly reaches a plateau around -0.1 V_{RHE}, in both RDE and proton pump setups. In the RDE experiment, this behaviour could be attributed to the rotation of the WE tip, which limits the maximum quantity of H_2 in contact with the catalyst layer. In the proton pump, the N_2 flushing removes most of the H_2 from the cathode compartment, only some H_2 remains in the direct surroundings of the catalyst layer or is trapped in its microstructure. It can be noted that the H_2 contribution is higher with Pt, most probably due to its higher activity towards HER.

To summarize, the fraction of H_{abs} reaches a maximum of 0.20 ± 0.02 in the PP and 0.47 ± 0.02 in the RDE setup. The N_2 flowing into the cathodic compartment of the PP is likely responsible for the lower value measured in this setup. However, the PP setup also allows the investigation of much lower voltages than in the RDE setup, i.e. < -0.5 V, which may be used advantageously in future studies. The oxidation of H_2 starts between 0.05–0 V vs RHE as could be expected, and this contribution is responsible for most of the increase in the H/Pd total below 0 V vs RHE.

Influence of the loading duration

The loading duration has been investigated in the range from 1 s to 5 min, at a constant loading potential of -0.1 V, in both the RDE and proton pump setups. Focus has been put on the short duration range, i.e. 1–10 s, to try to extract kinetics information related to the fast adsorption and absorption of hydrogen atoms onto and into Pd NPs.

First, a reference material containing Pt NPs has been investigated in the RDE setup. As the loading duration increases, a progressive rise of the overall current flowing during the desorption is observed (Figure 6(a)). The change is especially visible within the first five seconds, after which the current tends to stabilize, depicting that the saturation of the Pt surface with H is quickly reached. The modelling of the different contributions shows that the system is at equilibrium after about 10 s (Figure 6(d, g)). It can be noted that the maximum concentration of H_{ads} is lower than in the case of Pd NPs (Figure 6(e)), i.e. $H/Pt = 0.16 \pm 0.02$ vs $H/Pd = 0.18 \pm 0.02$, likely due to the difference in density of the two metals ($d_{Pt}/d_{Pd} \approx 1.8$), and therefore the number of particles for identical catalyst mass loadings. When compared relatively to this aspect, Pt NPs present a higher activity than Pd NPs towards the H adsorption, as could be expected.

In the case of Pd-based material, in the RDE setup, the desorption curves exhibit a clear trend towards the increase of the overall hydrogen atoms stored onto or into the catalyst layer (Figure 6(b)). The desorption of absorbed hydrogen, marked by a pronounced shoulder in the curve, significantly increases within the first seconds. The desorption of adsorbed hydrogen and the oxidation of H_2 follow a similar tendency, their contributions mainly impacting the very first points in the desorption curves. Calculations reveal that the increase in the amount of these three hydrogen species reaches a maximum after about 5 s of loading, after which their concentration is fairly constant (Figure 6(e, h)). It is unlikely that long loading durations can significantly improve the insertion of hydrogen atoms into the Pd lattice. The fast kinetics of H insertion into Pd NPs (under 5 s) is likely to be closely related to the NPs size. Earlier studies showed that the saturation of Pd thin films is achieved in a few seconds up to a few hours, depending on the film thickness.[21,32] For comparison, the NPs used in the present study exhibit a mean diameter of 3.8 ± 0.6 nm (Pd, cf. S.I. 1) and 3.8 ± 0.6 nm (Pt), as determined by transmission electron microscopy.

In the proton pump, changes occur within the first two to three seconds, after which the system is almost perfectly stable (Figure 6(c, f, i)). The maximum H_{ads}/Pd is similar to the one recorded in the RDE setup (≈ 0.18), showing a good accuracy of the model. As previously mentioned, the absorption of H is lower in the proton pump compared to the RDE setup, and long loading durations do not seem to enhance further the diffusion of H into the Pd lattice.

In brief, in comparison with Pd thin films commonly studied in the literature, the saturation of Pd NPs with H species is attained after a few seconds, i.e. approximately 5 s in the RDE setup and 3 s in the PP setup. Once at equilibrium, the composition of the Pd NPs is stable at does not significantly change even after 5 min at a potential of -0.1 V vs RHE.

Influence of the temperature

Temperature is expected to have a significant impact on the kinetics of the different reactions taking place during the hydrogen ads/absorption and desorption processes. This parameter has been studied in the RDE setup first, between 10–40 °C. Higher temperatures could not be reached due to technical limitations. All other experimental parameters were kept the same. The temperature was allowed to stabilize for 20 min before any measurement was performed. Examples of desorption curves recorded at four different temperatures, obtained after a loading step at -0.2 V_{RHE} for 60 s, are displayed in Figure 7(a). As could be expected, the desorption of hydrogen atoms gets faster as the temperature is increased, indicated by the desorption slope becoming steeper with increasing temperature. This result is in accordance with

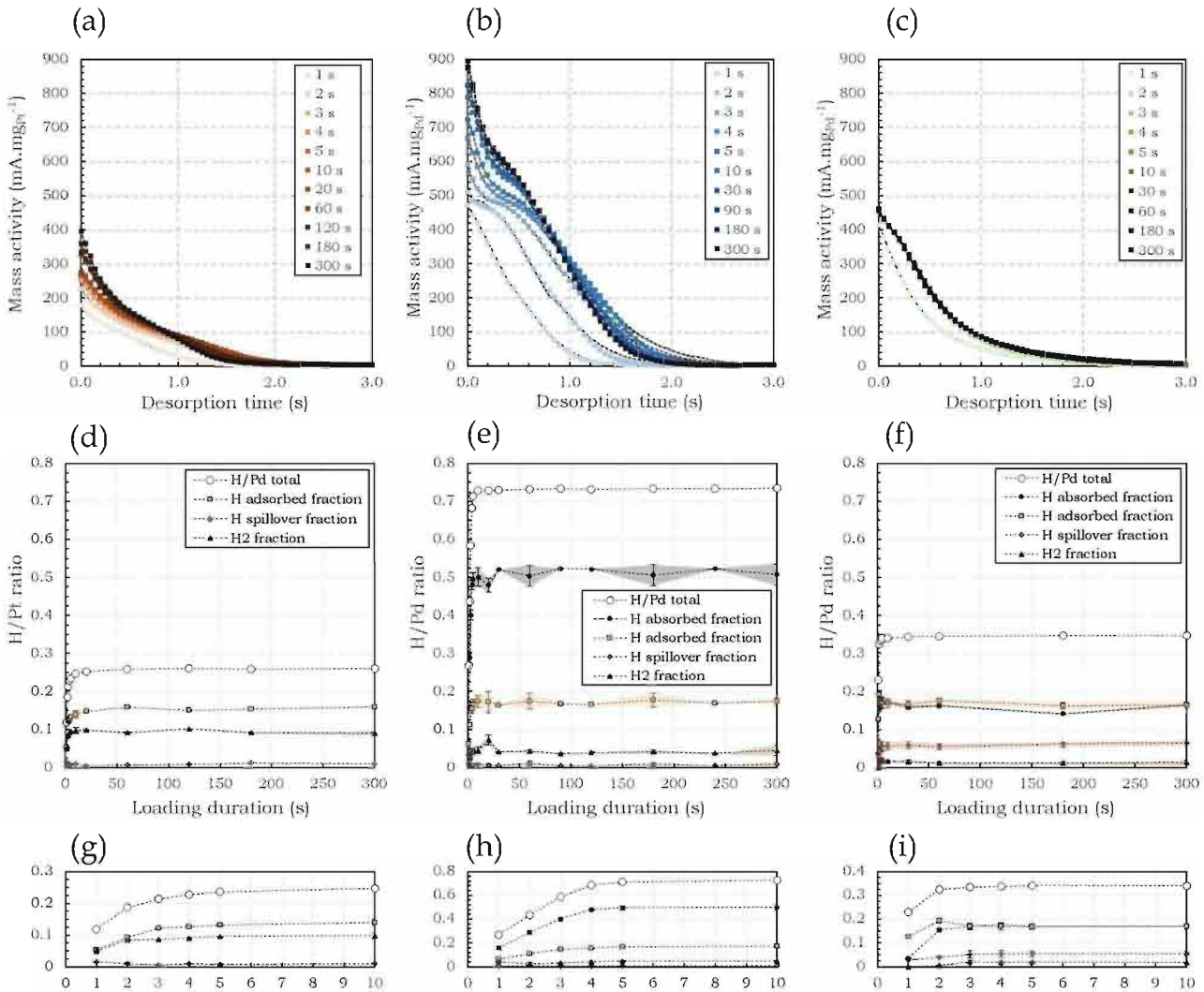

Figure 6. Electrochemical desorption curves recorded after loading at −0.1 V for the specified duration, desorption at + 0.4 V and calculated contributions of the different hydrogen species. (a, d) Pt/C-based catalyst material in the RDE setup (2500 rpm, 25 °C, H_2SO_4 0.5 M), (b, e) Pd/C-based catalyst material in the RDE setup (2500 rpm, 25 °C, H_2SO_4 0.5 M) and (c, f) $Pt_{(s)}/Pd_{(c)}$-based MEA in the proton pump setup (H_2 and N_2 flowrates 50 mL.min^{-1}, 30 °C). The dotted lines on the desorption curves correspond to the calculated model. Figures (g–i) are a close-up of the first ten seconds in figures (d – f).

previous studies on 0.9 ± 0.2 μm Pd–Au alloy films and 0.8 ± 0.1 μm Pd–Pt alloy films.[48,49] The modelling of the desorption curves (Figure 7(b–e)) reveals three main influences caused by the temperature: (i) an increase of the hydrogen absorption rates with temperature; (ii) a decrease of the hydrogen adsorption rates with increasing temperatures, for adsorption on palladium NPs and spillover on the carbon support alike, and (iii) a slightly larger evolution of H_2. This latter aspect is however limited by the maximum amount of H_2 that can be held on the WE, which causes all the H_2/Pd plots to plateau around H/Pd ratios of 0.07. Nonetheless, this plateau is reached for loading potentials of −0.2 V_{RHE} at 10 °C and −0.1 V_{RHE} at 40 °C.

From these results, it appears that hydrogen adsorption on Pd NPs and hydrogen spillover are closely related and follow the same trend. Cumulated H/Pd ratios at −0.3 V_{RHE} (H_{ads} + $H_{spillover}$) fall from 0.28 ± 0.02 at 10 °C to 0.14 ± 0.01 at 40 °C. This is in good agreement with the literature, as it is well known that hydrogen adsorption on various material surfaces is highly temperature dependent, high adsorption rates being reached at low temperatures.[50,51] In the meantime, the fraction of hydrogen atoms absorbed into the Pd structure increases with the temperature, from H/Pd ratios at −0.3 V_{RHE} of 0.32 ± 0.01 at 10 °C to 0.36 ± 0.01 at 30–40 °C. The larger diffusion rate of hydrogen atoms into the Pd NPs bulk is likely to be responsible for this variation as the hydrogen diffusivity in palladium is expected to increase with the temperature.[52] This shows the necessity of modelling the desorption curves into different contributions, as the evolution of the total H/Pd ratios with temperature, from 0.66 at 10 °C to 0.57 at 40 °C at −0.3 V_{RHE}, could be misinterpreted and lead to the conclusion that low temperatures enhance the absorption of hydrogen in Pd NPs.

It must be noted that no significant increment of the hydrogen absorption is visible between 30 °C and 40 °C (H_{abs}/Pd at −0.3 V_{RHE} of 0.37 ± 0.01 at 30 °C vs 0.36 ± 0.01 at 40 °C),

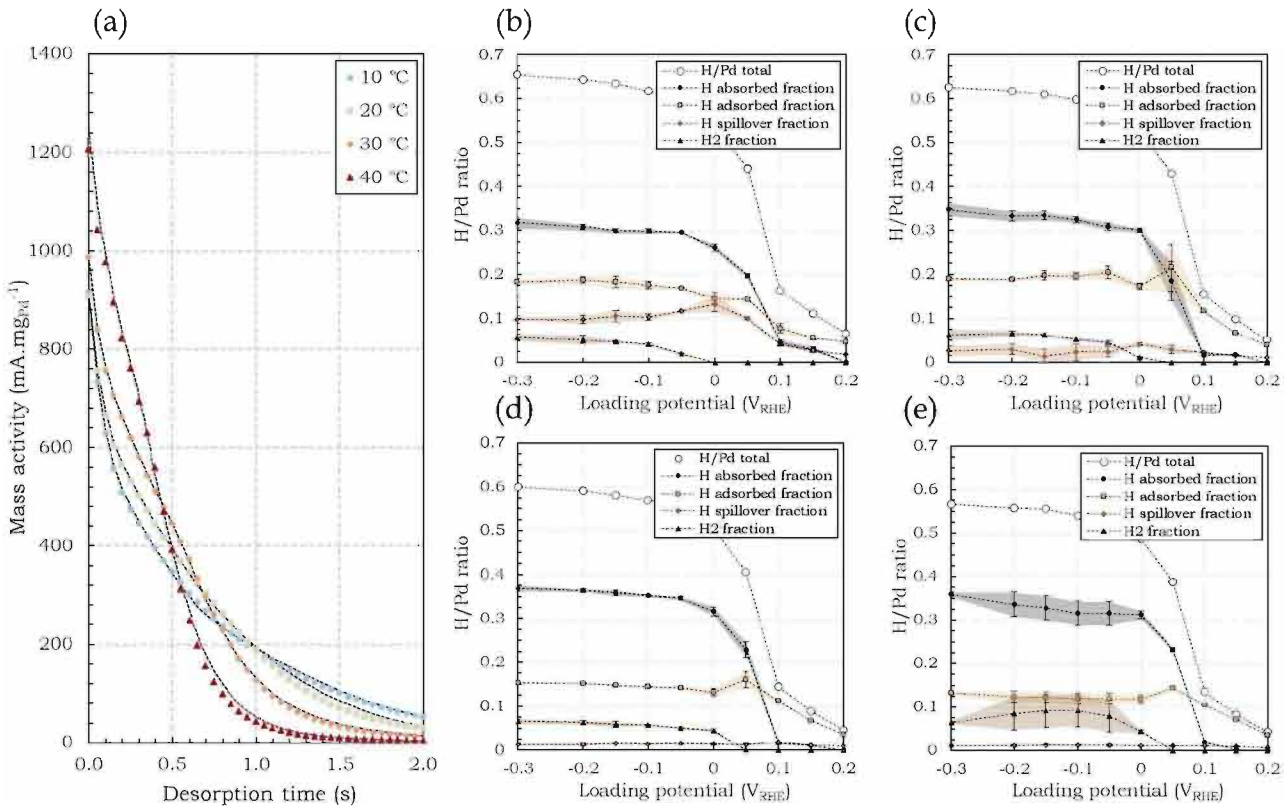

Figure 7. Electrochemical desorption curves recorded after 60 s loading at −0.2 V_{RHE}, desorption at +0.4 V_{RHE} (2500 rpm, H_2SO_4 0.5 M) (a) and modelling of the desorption curves at (b) 10 °C, (c) 20 °C, (d) 30 °C and (e) 40 °C. The dotted lines on the desorption curves correspond to the calculated model.

which could indicate an optimal temperature for the insertion of hydrogen into Pd around 30 °C. As H adsorption is the first step towards H absorption, it is likely that a low H adsorption rate participates to the decrease in the amount of H_{abs}. This effect will be further discussed in the proton pump setup, able to operate at higher temperatures.

The influence of the temperature was studied in the proton pump between 30–60 °C. The humidifiers' temperature was adjusted to keep a relative humidity close to 100%. The desorption curves (Figure 8(a)) present a net decrease in mass activity with the elevation of the temperature. Modellings exhibit with increasing temperatures (i) a continuous decrease in H_{ads}, as previously shown in the RDE setup, (ii) an increase in H_{abs} from 30 °C to 40 °C, followed by a decrease for higher temperatures and (iii) a shift of the transition from α-PdH_x to β-PdH_x towards lower cell voltages, also observed by Hubkowska *et al.*,[48,49] as well as a more gradual transition (Figure 8(b–e)). It should be noted that no contribution coming from H_{spill} was discernable and was therefore removed from the modelling.

The maximum amount of hydrogen absorption recorded at 40 °C for this series of measure (0.10 ± 0.01 at −0.5 V) confirm what seems to be an optimal temperature for the insertion of hydrogen into Pd. At lower temperatures, the diffusion of H from the Pd surface to the bulk might be too low to allow the saturation of the Pd lattice. Conversely, at a higher temperature, the quantity of H adsorbed on the Pd surface available to further diffuse into the Pd lattice might be too low to allow complete saturation. In their studies on Pd–Au films, Hubkowska *et al.* reported a constant decrease of the H absorbed contribution with increasing temperature (between 10 °C and 40 °C).[48] The authors stated that due to the exothermic behaviour of the H absorption into Pd, the reaction equilibrium shifts towards the hydride decomposition as the temperature is increased. The studied system is different from the one presented in this paper and this result is not in total accordance with our present observations, but it proposes another way to interpret the decrease of H_{abs} from 40 °C to 60 °C nonetheless.

The setup temperature also shows an influence on the H adsorption and absorption kinetics. As displayed in Figure 9, as the temperature increases, the reactions between H atoms and Pd NPs reach equilibrium after a longer time, from about 10 s at 30 °C to more than 30 s at 60 °C. This behaviour could be related to the lower H adsorption rate and higher HER reaction rate at the highest temperature investigated, greatly limiting the amount of H supplied at once for further diffusion into the Pd lattice.

In summary, in the studied range from 10–60 °C, the temperature has a very significant influence on the adsorption and absorption of H atoms onto and into Pd NPs. On one hand, the H_{ads} fraction constantly decreases with the increase in temperature, as expected from the literature. On the other hand, H_{abs} reaches a maximum at around 30–40 °C, which we believe can be attributed to a competitive effect between the

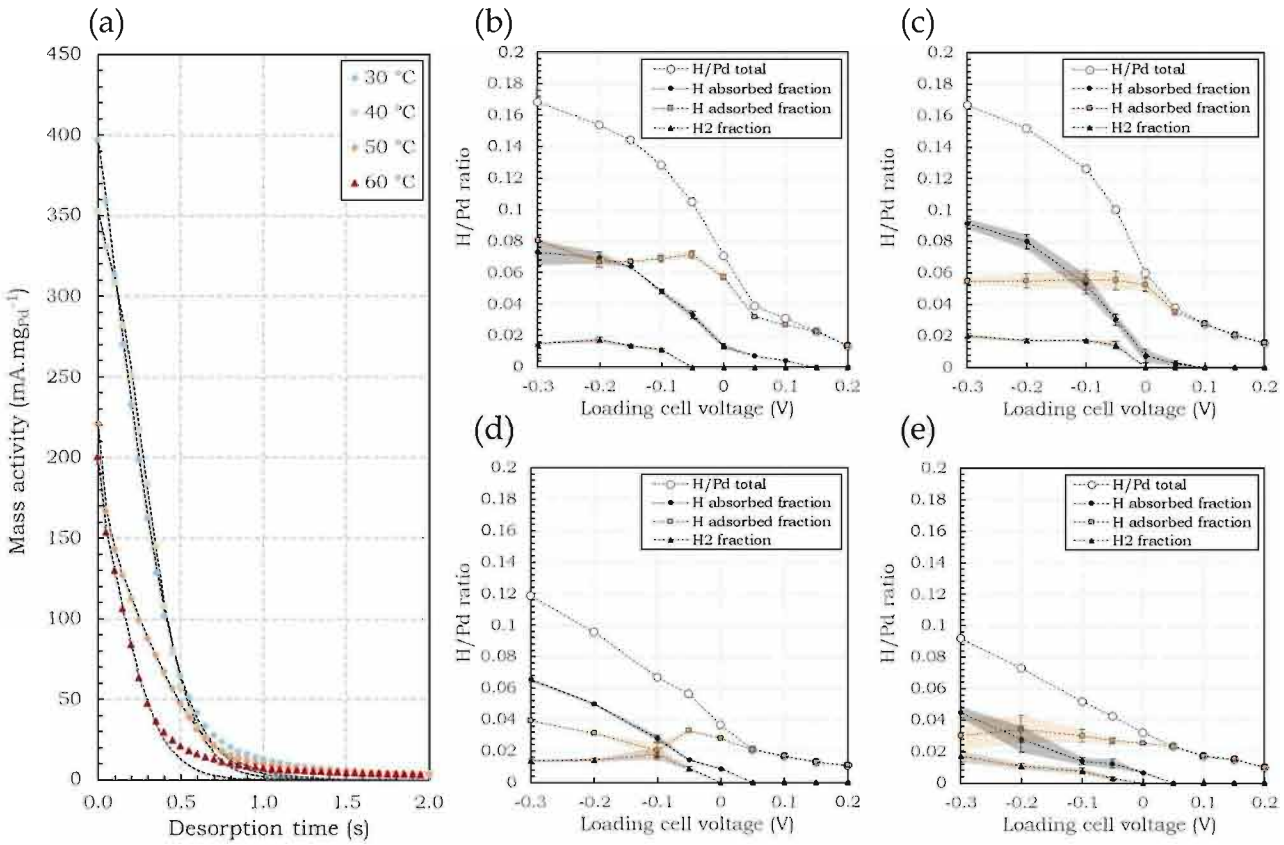

Figure 8. Electrochemical desorption curves recorded after 60 s loading at −0.2 V, desorption at +0.4 V (H_2 and N_2 flowrates 50 mL.min^{-1}) (a) and modelling of the desorption curves at (b) 30 °C, (c) 40 °C, (d) 50 °C and (e) 60 °C. The dotted lines on the desorption curves correspond to the calculated model.

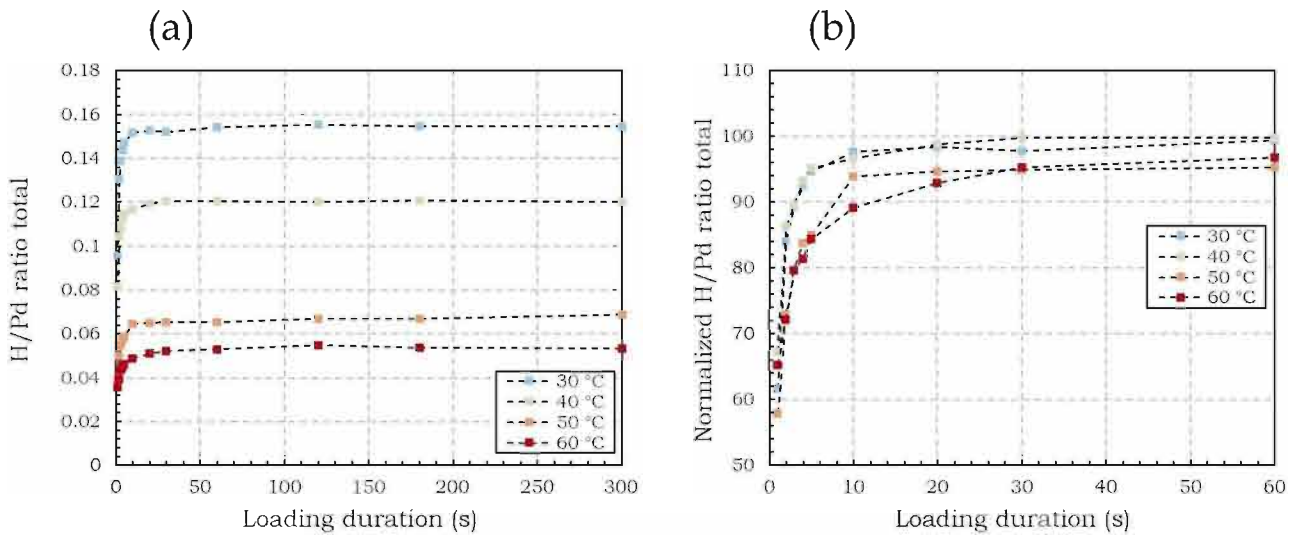

Figure 9. Integrations of the electrochemical desorption curves recorded after loading at −0.1 V for varied durations and at the specified temperatures, desorption at +0.4 V (H_2 and N_2 flowrates 50 mL.min^{-1}) (a), H/Pd ratio normalized with respect to the maximum ratio (b).

faster diffusion of H atoms into Pd NPs and the decreasing number of H_{ads} available to further diffuse into the Pd lattice with the increase in temperature. Additionally, it is observed that increasing the temperature slows down the establishment of the equilibrium between Pd and H, which might confirm our hypothesis.

Conclusion

The estimation of the amount of hydrogen atoms inserted into the Pd nanoparticles crystalline lattice can be achieved with simple electrochemical means. In the present publication, experiments have taken place in a three-electrode RDE setup and in a proton pump, leading to different kinetics and limitations. Two-step measurements have been carried out: first, the Pd-based catalyst layer is loaded with H atoms by applying a sufficiently low voltage, i.e. typically below $-0.1\ V_{RHE}$; then, a positive voltage is applied, and the desorption curve is recorded. A simple model based on the successive decays of hydrogen species has been proposed, allowing the separation of the contributions coming from hydrogen adsorption, absorption, spillover on the carbon support, and H_2 evolution. From this model, the variation of each individual contribution was determined with success and subsequently analysed.

In addition to the modelling, the influence on the hydrogen absorption of the loading voltage, loading duration and setup temperature have been investigated. From these results, the loading voltage was identified as having the largest impact on the H_{abs}/Pd, with values as high as 0.20 ± 0.02 in the proton pump and up to 0.47 ± 0.02 in the RDE setup. The transition from the α-PdH_x phase to the β-PdH_x phase was recorded between $0.1\ V_{RHE}$ and $0.05\ V_{RHE}$. Additionally, the model shows that hydrogen adsorption reaches a maximum around $0\ V_{RHE}$ and remains fairly constant for lower voltages. Below $0\ V_{RHE}$, most of the increase in the total H/Pd has been associated with H_2 oxidation. This result is of particular interest for electrocatalytic applications such as CO_2 reduction, where the quantity of H atoms absorbed into the Pd lattice influences greatly the product of the reaction.

The loading duration was found to have little influence on the H_{abs}/Pd ratio, in the range from 1 s to 300 s. After a few seconds of loading at $-0.1\ V_{RHE}$, about 5 s in the RDE setup and 2 s in the proton pump, the system reaches an equilibrium state. However, this study gives additional kinetics information on the reaction between protons and Pd NPs. If the contributions from hydrogen adsorption, absorption and H_2 evolution reach a maximum after a few seconds, the one from H spillover could present a faster increase once the Pd NPs surface is saturated. This trend should be confirmed by additional measurements. It is important to note that long loading durations do not seem to present any benefit for reaching high H/Pd ratio.

Finally, the setup temperature has been investigated between 10–40 °C in the RDE setup and 30–60 °C in the proton pump. In both setups, increasing temperatures lead to lower H_{ads}/Pd and $H_{spillover}$/Pd, in good agreement with the literature, while a maximal H_{abs}/Pd is found around 30–40 °C. This leads to the conclusion that in this temperature range, the H adsorption rate and the H diffusion rate into Pd might have attained an optimal balance. Furthermore, a slowing down of the adsorption and absorption kinetics is recorded as the temperature is increased, with equilibrium states being achieved in about 30 s at 60 °C. This result is of primary importance for research aiming at maximizing the quantity of H atoms absorbed into the Pd lattice, e.g. hydrogen storage or cold fusion-related studies.

Experimental section

Inks for the membrane electrode assemblies (MEAs) were prepared to reach a catalyst loading on both the anode and the cathode of $0.5\ mg_{Me}.cm^{-2}$ (Me = Pd or Pt), assuming a spraying efficiency of approximately 40%. The cathodic ink was prepared by mixing 35.9 mg of commercial Pd supported on Vulcan XC 72 (Premetek Co., 20 wt.%, 3.8 ± 0.6 nm, cf. S.I. 1), 71.9 µL of milli-Q water ($18.2\ M\Omega.cm^{-1}$) and 395 µL of iso-propanol (Honeywell, Chromasolv, ≥99.9%). After stirring for 10 min on a magnetic stirrer, 280 µL of a Nafion solution (Sigma-Aldrich, 5 wt.%) was added. The ink was finally stirred for 30 min, followed by a 10-minute sonication. The same procedure was used for the anodic ink, using 32.1 mg of commercial Pt supported on carbon black (Alfa Aesar, 20 wt.%, 3.8 ± 0.6 nm) and 96.3 µL, 385.2 µL and 250.1 µL of milli-Q water, iso-propanol and Nafion dispersion, respectively. The inks were stirred until further used.

MEAs were prepared by spraying the catalyst inks on both sides of a 20 cm^2 Nafion membrane 115 (Ion Power), using a square pattern of 5.29 cm^2. The membrane was dried for 2 h at 180 °C in a vacuum oven (Heraeus) and weighed prior to the first spraying and after each spraying to measure the actual catalyst loading on each side of the membrane. The MEA was stored in milli-Q water for at least 18 h before being introduced in the fuel cell (Fuel Cell Technology, Inc.).

The fuel cell was used in a proton pump mode at 30 °C (unless specified otherwise) H_2 (AGA, 5.0) was fed at the anode side ($50\ mL.min^{-1}$), and N_2 (5.0) was flushing the cathode side ($50\ mL.min^{-1}$). Both gases were humidified (100%) before entering the cell. The gas pressure in the cell is equal to atmospheric pressure. Measurements were carried out with an Autolab potentiostat (PGSTAT100) and recorded with the software Nova.

Inks for the RDE analysis were prepared by mixing 5 mg of commercial Pd/C (Premetek Co., 20 wt.%) or Pt/C (Alfa Aesar, 20 wt.%) with 100 µL of milli-Q water, 100 µL of ethanol (Altia Oyj, 99.5%) and 20 µL of Nafion solution (Sigma-Aldrich, 5 wt.%). The mixture was then stirred for 15 min and sonicated for 30 min. The inks were stirred until further used.

The working electrode (WE) used in the RDE setup is a glassy carbon tip of 0.196 cm^2. 5 µL of the catalyst ink was deposited on its surface, corresponding to a loading of $0.12\ mg_{Me}.cm^{-2}$. The WE was then dipped into water for 12–18 h to mitigate the hydrophobic nature of the catalyst layer, assuring the quick and efficient removal of evolved H_2 bubbles during the measurements.

The WE was placed on a rotator (Pine MSRX speed control) and introduced in a glass cell. Measurements were carried out in 0.5 M H_2SO_4 electrolyte (Merck, Titripur®) at 25 °C. The reference electrode was a reversible hydrogen electrode (RHE) (Gaskatel, Hydroflex®) and the counter electrode (CE) was an iridium wire, cleaned and polished before use. The analysis were performed using an Autolab potentiostat (PGSTAT128N) controlled by the software Nova.

Hydrogen electrochemical loading and desorption measurements were carried out in two steps: (i) a constant voltage (potential) is applied to the proton pump (WE) for a determined duration; (ii) the desorption of hydrogen atoms is achieved by applying a voltage of +0.4 V to the proton pump (or $+0.4\ V_{RHE}$ to the WE) for

60 s, long enough to reach an almost null current. In the case of proton pump experiments, a small positive current (0.4–0.8 mA.cm^{-2}) is always present during the desorption step due to dihydrogen crossover through the Nafion membrane, resulting in the oxidation of dihydrogen into protons. This contribution was removed by averaging this positive current during the last 10 s and subtracting it from the whole curve.

Potential controlled electrochemical impedance spectroscopy (EIS) measures were performed after 20 min stabilization at the set voltage, using 20 mV amplitude in the frequency range from 10 kHz to 100 mHz. Collected data were modelled with a model composed of an ohmic resistance R_{ohm} in series with two identical subcircuits, both containing a resistance R_{ct} (charge transfer resistance) in parallel with a CPE. An additional resistance R_{mt} (mass transfer resistance) in parallel with a capacitor C_{mt} were added to model the mass transfer contribution appearing at low voltages. Using the circuit description code proposed by Boukamp,[53] the equivalent circuit can be written: R_{ohm} ($R_{ct,a}$ CPE_a) ($R_{ct,c}$ CPE_c) (R_{mt} C_{mt}). Subscript letters *a* and *c* indicate elements related to the anodic and cathodic sides respectively.

CRediT author statement

Lilian Moumaneix: Conceptualization, Methodology, Formal analysis, Investigation, Writing – Original Draft, Writing – Review & Editing, Visualization. **Akseli Rautakorpi**: Investigation, Writing – Review & Editing. **Tanja Kallio**: Conceptualization, Writing – Review & Editing, Supervision, Funding acquisition

Acknowledgements

This project has received funding from the European Union's Horizon 2020 research and innovation program under grant agreement N° 952184 (HERMES project).

Conflict of Interest

The authors declare no conflict of interest.

Data Availability Statement

The data used in the present study are available using the following link: https://etsin.fairdata.fi/dataset/83a9e81d-a3c9-41e8-972a-32a537c96b02.

Keywords: Absorption · Desorption curve modelling · Hydride · Palladium nanoparticles · Proton pump

[1] S. Dekura, H. Kobayashi, K. Kusada, H. Kitagawa, *ChemPhysChem* **2019**, *20*, 1158–117.
[2] S. K. Konda, A. Chen, *Mater. Today* **2016**, *19*, 100–108.
[3] M. Yamauchi, R. Ikeda, H. Kitagawa, M. Takata, *J. Phys. Chem. C* **2008**, *112*, 3294–3299.
[4] R. Checchetto, N. Bazzanella, B. Patton, A. Miotello, *Surf. Coat. Technol.* **2004**, *177–178*, 73–79.
[5] Z. W. Dunbar, *J. Power Sources* **2015**, *297*, 525–533.
[6] M. R. Rahimpour, F. Samimi, A. Babapoor, T. Tohidian, S. Mohebi, *Chem. Eng. Process.* **2017**, *121*, 24–49.
[7] M. Yuan, K, Lee, D. G. Van Campen, S. Liguori, M. F. Toney, J. Wilcox, *Ind. Eng. Chem. Res.* **2019**, *58*, 926–934.
[8] N. A. Al-Mufachi, N. V. Rees, R. Steinberger-Wilkens, *Renewable Sustainable Energy Rev.* **2015**, *47*, 540–551.
[9] I. Darmadi, F. A. A. Nugroho, C. Langhammer, *ACS Sens.* **2020**, *5*, 3306–3327.
[10] G. Behzadi Pour, L. Fekri Aval, M. Nasiri Sarvi, S. Fekri Aval, H. Nazarpour Fard, *J. Mater. Sci. Mater. Electron.* **2019**, *30*, 8145–8153.
[11] C. C. Ndaya, N. Javahiraly, A. Brioude, *Sensors* **2019**, *19*, 4478.
[12] E. Antolini, *Energy Environ. Sci.* **2009**, *2*, 915–931.
[13] L. Zhang, Q. Chang, H. Chen, M. Shao, *Nano Energy* **2016**, *29*, 198–219.
[14] J. Calderón Gómez, R. Moliner, M. Lázaro, *Catalysts* **2016**, *6*, 130.
[15] T. Skośkiewicz, *Phys. Status Solidi B* **1973**, *59*, 329–334.
[16] G. Jerkiewicz, *Prog. Surf. Sci.* **1998**, *57*, 137–186.
[17] S. M. Kozlov, H. A. Aleksandrov, K. M. Neyman, *J. Phys. Chem. C* **2014**, *118*, 15242–15250.
[18] C. Gabrielli, P. P. Grand, A. Lasia, H. Perrot, *J. Electrochem. Soc.* **2004**, *151*, A192S–A1936.
[19] A. Lasia, in *Electrochemical impedance spectroscopy and its applications*, Springer, **2014**.
[20] R. Crețu, A. Kellenberger, N. Vaszilcsin, *Int. J. Hydrogen Energy* **2013**, *38*, 11685–11694.
[21] L. Birry, A. Lasia, *Electrochim. Acta* **2006**, *51*, 3356–3364.
[22] P. Tripodi, D. Di Gioacchino, J. D. Vinko, *J. Alloys Compd.* **2009**, *486*, 5S–59.
[23] G. Bambakidis, R. J. Smith, D. A. Otterson, *Phys. Rev.* **1969**, *177*, 1044–1048.
[24] A. Rose, S. Maniguet, R. J. Mathew, C. Slater, J. Yao, A. E. Russell, *Phys. Chem. Chem. Phys.* **2003**, *5*, 3220.
[25] B. Baranowski, R. Wiśniewski, *Phys. Status Solidi B* **1969**, *35*, 593–597.
[26] W.-S. Zhang, Z.-F. Zhang, Z.-L. Zhang, *J. Electroanal. Chem.* **2002**, *528*, 1–17.
[27] M. C. H. McKubre, F. L. Tanzella, *J. Condens. Matter Nucl. Sci.* **2006**, 392–403.
[28] D. R. Lawson, M. J. Tierney, I. F. Cheng, L. S. Van Dyke, M. W. Espenscheid, C. R. Martins, *Electrochim. Acta* **1991**, *36*, 1515–1522.
[29] R. Chattot, I. Martens, M. Mirolo, M. Ronovsky, F. Russello, H. Isern, G. Braesh, E. Hornberger, P. Strasser, E. Sibert, M. Chatenet, V. Honkimäki, J. Drnec, *J. Am. Chem. Soc.* **2021**, *143*, 17068–17078.
[30] J. D. Benck, A. Jackson, D. Young, D. Rettenwander, Y.-M. Chiang, *Chem. Mater.* **2019**, *31*, 4234–4245.
[31] C. P. Berlinguette, Y.-M. Chiang, J. N. Munday, T. Schenkel, D. K. Fork, R. Koningstein, M. D. Trevithick, *Nature* **2019**, *570*, 45–51.
[32] R. P. Jansonius, P. A. Shauer, D. J. Dvorak, B. P. MacLeod, D. K. Fork, C. P. Berlinguette, *Angew. Chem. Int. Ed.* **2020**, *59*, 12192–12198; *Angew. Chem.* **2020**, *132*, 12290–12296.
[33] R. S. Sherbo, M. Moreno-Gonzalez, N. J. J. Johnson, D. J. Dvorak, D. K. Fork, C. P. Berlinguette, *Chem. Mater.* **2018**, *30*, 3963–3970.
[34] A. Czerwinski, I. Kiersztyn, M. Grden, J. Czapla, *J. Electroanal. Chem.* **1999**, *471*, 190–19S.
[35] C. Gabrielli, P. P. Grand, A. Lasia, H. Perrot, *J. Electrochem. Soc.* **2004**, *151*, A1937–A1942.
[36] P. N. Bartlett, B. Gollas, S. Guerin, J. Marwan, *Phys. Chem. Chem. Phys.* **2002**, *4*, 3835–3842.
[37] H. Duncan, A. Lasia, *Electrochim. Acta* **2008**, *53*, 6845–6850.
[38] M. H. Martin, A. Lasia, *Electrochim. Acta* **2008**, *53*, 6317–6322.
[39] A. Czerwiński, S. Zamponi, R. Marassi, *J. Electroanal. Chem. Interfacial Electrochem.* **1991**, *304*, 233–239.
[40] M. Łukaszewski, K. Kuśmierczyk, J. Kotowski, H. Siwek, A. Czerwiński, *J. Solid State Electrochem.* **2003**, *7*, 69–76.
[41] R. J. Behm, K. Christmann, G. Ertl, *Surf. Sci.* **1980**, *99*, 320–340.
[42] M. Nordio, F. Rizzi, G. Manzolini, M. Mulder, L. Raymakers, M. Van Sint Annaland, F. Gallucci, *Chem. Eng. J.* **2019**, *369*, 432–442.
[43] B. Rohland, K. Eberle, R. Ströbel, J. Scholta, J. Garche, *Electrochim. Acta* **1998**, *43*, 3841–3846.
[44] Y. M. Hao, H. Nakajima, A. Inada, K. Sasaki, K. Ito, *Electrochim. Acta* **2019**, *301*, 274–283.
[45] A. Huth, B. Schaar, T. Oekermann, *Electrochim. Acta* **2009**, *54*, 2774–2780.
[46] O. Sorsa, J. Nieminen, P. Kauranen, T. Kallio, *J. Electrochem. Soc.* **2019**, *166*, F1326–F1336.

[47] M.-T. Nguyen, S. A. Grigoriev, A. A. Kalinnikov, A. A. Filippov, P. Millet, V. N. Fateev, *J. Appl. Electrochem.* **2011**, *41*, 1033–1042.
[48] K. Hubkowska, M. Łukaszewski, A. Czerwiński, *Electrochim. Acta* **2010**, *56*, 235–242.
[49] K. Hubkowska, M. Łukaszewski, A. Czerwiński, *Electrochim. Acta* **2011**, *56*, 2344–2350.
[50] K. M. Thomas, *Catal. Today* **2007**, *120*, 389–398.
[51] R. Gómez, J. M. Orts, B. Álvarez-Ruiz, J. M. Feliu, *J. Phys. Chem. B* **2004**, *108*, 228–238.
[52] Y. Li, G. Wahnström, *Phys. Rev. B* **1992**, *46*, 14528–14542.
[53] B. A. Boukamp, Equivalent circuit users manual, 2nd revised edition, Department of Chemistry, Technical University of Twente.

Manuscript received: November 21, 2022
Revised manuscript received: January 12, 2023